Shape optimisation of the energy efficiency of building retrofitted facade

Sultan ALPAR [1]*, **Julien BERGER** [1], **Rafik BELARBI** [1]

[1]Laboratoire des Sciences de l'Ingénieur pour l'Environnement (LaSIE), UMR 7356 CNRS, La Rochelle Université, CNRS, 17000, La Rochelle, France
*(Corresponding author: sultan.alpar@univ-lr.fr)

Abstract - This article deals design optimization of building walls. The boundary element method is used to solve the problem due to its computational efficiency and accuracy. For a case study in summer and winter configuration, the optimal shape of the outside boundary of the wall is retrieved. It enables to increase significantly the energy efficiency compared to the flat wall.

Nomenclature

T	temperature, $[\,\mathrm{K}\,]$	k	heat conductivity , $[\,\mathrm{W}\,.\,\mathrm{m}^{-1}\,.\,\mathrm{K}^{-1}\,]$
x	horizontal space coordinate , $[\,\mathrm{m}\,]$	γ	boundary shape function , $[\,\mathrm{m}\,]$
y	vertical space coordinate , $[\,\mathrm{m}\,]$	Γ	boundary , $[\,-\,]$
H	building facade height , $[\,\mathrm{m}\,]$	ρ	dimensionless flux , $[\,-\,]$
L	thickness of the wall , $[\,\mathrm{m}\,]$	Φ	fundamental solution , $[\,-\,]$
q_L	incident radiation flux , $[\,\mathrm{W}\,.\,\mathrm{m}^{-2}\,]$	r	distance , $[\,-\,]$

1. Introduction

Due to their environmental impacts, retrofit existing building is a crucial challenge for designers. It requires an accurate prediction of the heat losses through the multi-layers walls to propose energy efficient strategies. The challenge is even more important when considering the thermal stresses due to climate change warming temperature and solar radiation. Buildings retrofitted today must adapt to future extreme heat is crucial. However, despite all the building simulation programs developed for the past 50 years, the building wall are often designed under the following assumption. The walls are plane barriers created against the climatic varying outside conditions. It omits the fact that incident radiation heat flux are not spread uniformly on the enclosure [1]. The scientific issue is the following: can the energy efficiency be increased by carrying shape optimization of the wall? As mentioned in [2], new numerical methods are required for the design of advanced wall with improved energy efficiency. In this article, the boundary element method is developed to solve the two-dimensional steady state heat transfer equation in walls with spatial varying incident flux. The method is then used to solve the design problem to determine the optimal shape that increase the energy efficiency of the wall.

2. Mathematical model

2.1. Physical problem

The physical domain under investigations is illustrated in Figure 1. The domain is denoted by Ω with space coordinates $\boldsymbol{x} = \big(x\,,\,y\big)$. The height of the facade is $H\,\big[\,\mathrm{m}\,\big]$. The boundary of the domain is $\Gamma = \cup_{i=1}^{4}\,\Gamma_i$. The bottom, right and top boundaries are denoted as Γ_2, Γ_3 and Γ_4, respectively. The left boundary is Γ_1 and is defined by:

$$\Gamma_1(\boldsymbol{p}) = \{\,\boldsymbol{x} \in \mathbb{R}^2 \,|\, x = \gamma\,(\boldsymbol{p}\,,\,y)\,,\, y \in [\,0\,,\,H]\,,\, \boldsymbol{p} \in \Omega_p\}\,, \tag{1}$$

https://doi.org/10.25855/SFT2023-039

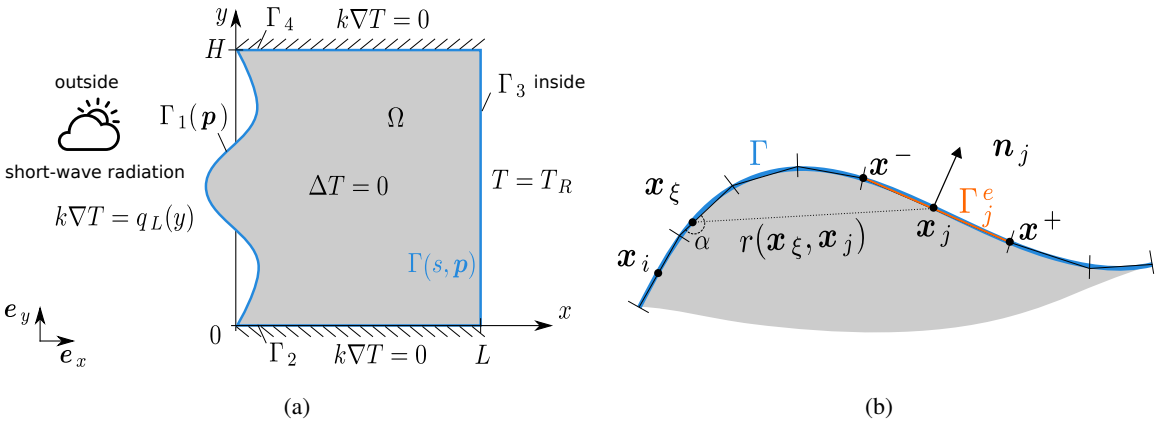

Figure 1 : *Illustration of the physical problem* (a). *Illustration of the approximation of the whole boundary* Γ (b).

where $\gamma(\boldsymbol{p}, y)$ is a parametrized mapping function, which shapes the form of the boundary Γ_1 depending on the N_p parameters:

$$\boldsymbol{p} = (p_1, \ldots, p_{N_p}) \in \Omega_p .$$

Note that in the case $\gamma(\boldsymbol{p}, y) = 0$, we have a plane boundary Γ_1 and the facade is a classical rectangular one. In such case, the length of the wall is denoted $L\ [\mathrm{m}]$.

The two-dimensional steady-state heat diffusion transfer is assumed to represent the physical phenomena in the building facade [3]:

$$\boldsymbol{\Delta} T = 0, \qquad \forall \boldsymbol{x} \in \Omega,$$

where $T\ [\mathrm{K}]$ is the temperature inside the facade. The left boundary is in contact with the outside environment of the building. A second-type boundary condition is assumed where the flux $q\ [\mathrm{W.m^{-2}}]$ corresponds to the incident short-wave solar radiation:

$$k\, \boldsymbol{\nabla} T\, \vec{n} = q_L(\boldsymbol{x}), \qquad \forall \boldsymbol{x} \in \Gamma_1,$$

where $k\ [\mathrm{W.m^{-1}.K^{-1}}]$ is the thermal conductivity of the wall. Also note that the incident flux q_L varies with the height of the facade due to the surrounding effects of the urban area and due to the shape of the boundary that may induce local shadings. It is given by:

$$q_L(\boldsymbol{x}) = \beta(q^{\mathrm{dr}}(\boldsymbol{x}) + q^{\mathrm{df}}(\boldsymbol{x}) + q^{\mathrm{rf}}(\boldsymbol{x})),$$

where direct $q^{\mathrm{dr}}\ [\mathrm{W.m^{-2}}]$, diffusive $q^{\mathrm{df}}\ [\mathrm{W.m^{-2}}]$ and reflective $q^{\mathrm{rf}}\ [\mathrm{W.m^{-2}}]$ fluxes are components of the incident short-wave radiation. β is the absorptivity of the wall.

The right boundary is in contact with the ambient air so a DIRICHLET boundary condition is assumed:

$$T = T_R, \qquad \forall \boldsymbol{x} \in \Gamma_3,$$

where T_R is the known inside ambient temperature. Last, the top and bottom boundaries of the facade are assumed as adiabatic:

$$k\, \boldsymbol{\nabla} T\, \vec{n} = 0, \qquad \forall \boldsymbol{x} \in \Gamma_2 \cup \Gamma_4 .$$

2.2. Dimensionless formulation

The space, time and temperature quantities are transformed into a dimensionless representation according to:

$$\boldsymbol{x}^\star \;=\; \left(x^\star\,,\,y^\star\right), \quad x^\star \;=\; \frac{x}{H}\,, \quad y^\star \;=\; \frac{y}{H}\,, \quad u \;=\; \frac{T}{T_R}\,.$$

With this transformations, the dimensionless problem is set on the new domain $\Omega^\star$ and the left boundary Γ_1 is now redefined as:

$$\Gamma_1^\star(\,\boldsymbol{p}^\star\,) \;=\; \{\,\boldsymbol{x}^\star \,|\, x^\star \;=\; \gamma^\star\,(\,\boldsymbol{p}^\star\,,\,y^\star)\,,\, y^\star \;\in\; [\,0\,,\,1\,]\,,\, \boldsymbol{p}^\star \;\in\; \Omega_p^\star\}\,.$$

Then, the governing equations is:

$$\boldsymbol{\Delta}^\star u \;=\; 0\,, \tag{2}$$

with the boundary conditions:

$$\begin{aligned} \nabla^\star u\,\vec{n} \;&=\; \rho(\boldsymbol{x}^\star)\,, && \boldsymbol{x}^\star \in \Gamma_1\,,\\ \nabla^\star u\,\vec{n} \;&=\; 0\,, && \boldsymbol{x}^\star \in \Gamma_2 \cup \Gamma_4\,,\\ u \;&=\; 1\,, && \boldsymbol{x}^\star \;\in\; \Gamma_3\,. \end{aligned}$$

where $\rho(\boldsymbol{x}^\star) \;=\; \frac{q_L\,(\,\boldsymbol{x}\,)\,H}{k\,T_R}$.

2.3. Numerical method to solve the direct problem

2.3.1. Boundary Integral equation

To derive the boundary integral equation of Eq. (2), we use GREEN's second identity for two regular functions:

$$\int_{\Omega\,-\,\Omega\epsilon} \left(\,u\,\nabla^2\,\Phi^\star \;-\; \Phi^\star\,\nabla^2\,u\,\right)\,dV \;=\; \int_\Gamma \left(\,u\,q^\star \;-\; \Phi^\star\,q\,\right)\,d\Gamma \;+\; \int_{\Gamma_\epsilon} \left(\,u\,q^\star \;-\; \Phi^\star\,q\,\right)\,d\Gamma_\epsilon, \tag{3}$$

where u is solution of our dimensionless problem defined for the bounded two-dimensional region Ω with its closed boundary curve Γ. $\Phi^\star$ is the fundamental solution of LAPLACE's equation for the bounded two-dimensional region Ω_ϵ with its closed boundary curve Γ_ϵ. q and $q^\star$ are normal derivatives for u and $\Phi^\star$:

$$q \;=\; \nabla^\star u\,\vec{n}\,, \qquad q^\star \;=\; \nabla^\star \Phi^\star\,\vec{n}.$$

Last, $\Phi^\star$ is defined by :

$$\Phi^\star \;=\; -\,\frac{\ln\,(\,r\,)}{2\,\pi\,(\,R_1\,R_2)^{1/2}},$$

where r is the distance from a source point to a boundary point, which is defined as:

$$r \;=\; \left[\,\frac{1}{R_1}\,(\,x^\star - x_\xi)^2 \;+\; \frac{1}{R_2}\,(\,y^\star - y_\xi)^2\,\right]^{1/2},$$

here $\boldsymbol{x}_\xi \;=\; (\,x_\xi\,,\,y_\xi\,)$ is a source point coordinates and $\boldsymbol{x} \;=\; (x^\star,\,y^\star)$ is a boundary point coordinates, which is shown in Figure 1(b).

u and $\Phi^\star$ satisfy LAPLACE's equation in the new region $\Omega \;-\; \Omega\epsilon$, thus the domain integral is equal to zero. The original region is recovered on taking the limit when $\epsilon \;\to\; 0$. The limit of the second integral on the right-hand side over Γ_ϵ in Eq. (3) produces the result:

$$\lim_{\epsilon\,\to\,0} \int_{\Gamma_\epsilon} \left(\,u\,(\boldsymbol{x})\,q^\star(\boldsymbol{x}_\xi,\,\boldsymbol{x}) \;-\; \Phi^\star(\boldsymbol{x}_\xi,\,\boldsymbol{x})\,q\,(\boldsymbol{x})\,\right)\,d\Gamma_\epsilon \;=\; u(\boldsymbol{x}_\xi)\,,$$

and the following integral equation is obtained from Eq. (3):

$$u(\boldsymbol{x}_\xi) \;=\; \int_\Gamma \Big(\Phi^\star(\boldsymbol{x}_\xi,\, \boldsymbol{x})\, q\,(\boldsymbol{x}) \;-\; u\,(\boldsymbol{x})\, q^\star(\boldsymbol{x}_\xi,\, \boldsymbol{x}) \Big)\, d\Gamma, \tag{4}$$

this equation is known as GREEN's third identity.

To obtain a boundary integral equation relating only boundary values, the limit is taken when the point $\boldsymbol{x}_\xi$ tends to a point $\boldsymbol{x}$ on the boundary Γ. However, if $\boldsymbol{x}_\xi$ belongs to the boundary Γ. The limits produce what is called a free term. Taking into account these terms the boundary integral equation Eq. (4) can be generalized in the form:

$$c(\boldsymbol{x}_\xi)\, u(\boldsymbol{x}_\xi) \;=\; \int_\Gamma \Big(\Phi^\star(\boldsymbol{x}_\xi,\, \boldsymbol{x})\, q\,(\boldsymbol{x}) \;-\; u\,(\boldsymbol{x})\, q^\star(\boldsymbol{x}_\xi,\, \boldsymbol{x}) \Big)\, d\Gamma, \tag{5}$$

for any point $\boldsymbol{x}_\xi$ on the boundary Γ. The free coefficient $c(\boldsymbol{x}_\xi)$ is given by:

$$c(\boldsymbol{x}_\xi) \;=\; \frac{\alpha}{2\,\pi}\,, \qquad 0 \;\leq c(\boldsymbol{x}_\xi) \leq 1,$$

where α is an internal angle at source point $\boldsymbol{x}_\xi$.

2.3.2. Discrete Boundary Integral equation

The Boundary integral equation (BIE) Eq. (5) can only be solved analytically for some very simple problems. For this, a standard GREEN's function method is normally used. Rather than attempting analytical solutions to the BIE for particular geometries and boundary conditions, we seek a suitable reduction of the equation to an algebraic form that can be solved by a numerical approach.

The Boundary element method (BEM) is a numerical method of solution of the BIE, based on a discretization procedure [4]. Application requires two types of approximation: the first geometrical, involving a subdivision of the boundary Γ into N_e small segments or elements Γ_j, schematically shown in Figure 1(b), such that:

$$\sum_{j=1}^{N_e} \Gamma_j \approx\; \Gamma,$$

Taking this into account, Eq. (5) can be written in the form:

$$c(\boldsymbol{x}_\xi)\, u(\boldsymbol{x}_\xi) \;=\; \sum_{j=1}^{N_e} \int_{\Gamma_j} \Big(\Phi^\star(\boldsymbol{x}_\xi,\, \boldsymbol{x})\, q\,(\boldsymbol{x}) \;-\; u\,(\boldsymbol{x})\, q^\star(\boldsymbol{x}_\xi,\, \boldsymbol{x}) \Big)\, d\Gamma, \tag{6}$$

The second approximation required by the BEM is functional. We approximate the variation of u and q within each element by writing them in terms of their values at some fixed points in the element, using interpolation functions. The simplest possible approximation is a piecewise constant one, which assumes that u and q are constant within each element and equal to their value at the midpoint. Using this approximation into Eq. (6), we obtain:

$$c(\boldsymbol{x}_i)\, u(\boldsymbol{x}_i) \;=\; \sum_{j=1}^{N_e} q\,(\boldsymbol{x}_j) \int_{\Gamma_j} \Phi^\star(\boldsymbol{x}_i,\, \boldsymbol{x})\, d\Gamma \;-\; u\,(\boldsymbol{x}_j) \int_{\Gamma_j} q^\star(\boldsymbol{x}_i,\, \boldsymbol{x})\, d\Gamma, \tag{7}$$

here i - nodal point, j - number of the element. Calling integrals

$$G_{i\,j} \;=\; \int_{\Gamma_j} \Phi^\star(\boldsymbol{x}_i,\, \boldsymbol{x})\, d\Gamma \tag{8}$$

and

$$\hat{H}_{ij} = \int_{\Gamma_j} q^\star(\boldsymbol{x}_i, \boldsymbol{x})\, d\Gamma\,, \qquad H_{ij} = \hat{H}_{ij} + c(\boldsymbol{x}_i)\,\delta_{ij}, \tag{9}$$

where δ_{ij} is the Kronecker delta.

Integration in Eq. (8) and (9) is carried out using composite SIMPSON's rule. Quadratic boundary elements are used to represent curved geometry. Thus the Jacobian and normal vector are no longer constant within each element. In order to implement them, there is a need to transform from Cartesian to curvilinear coordinates [5]. For the sake of brevity, transformation omitted by authors.

Now Eq. (7) can be rewritten in the form:

$$\sum_{j=1}^{N_e} H_{ij}\, u_j = \sum_{j=1}^{N_e} G_{ij}\, q_j, \tag{10}$$

for any nodal point i. If the above equations are now applied, this generates a system of equations which can be written in matrix form as:

$$\underline{\underline{\boldsymbol{H}}}\,\underline{\boldsymbol{u}} = \underline{\underline{\boldsymbol{G}}}\,\underline{\boldsymbol{q}}. \tag{11}$$

Once the boundary conditions of the problem are applied to the system of Eq. (11), the matrices can be reordered in the form:

$$\underline{\underline{\boldsymbol{A}}}\,\underline{\boldsymbol{x}} = \underline{\boldsymbol{b}}, \tag{12}$$

in which all unknowns have been collected into the vector $\underline{\boldsymbol{x}}$, and the vector $\underline{\boldsymbol{b}}$ is the 'load' vector, which contains all known boundary conditions.

2.4. Verification of BEM

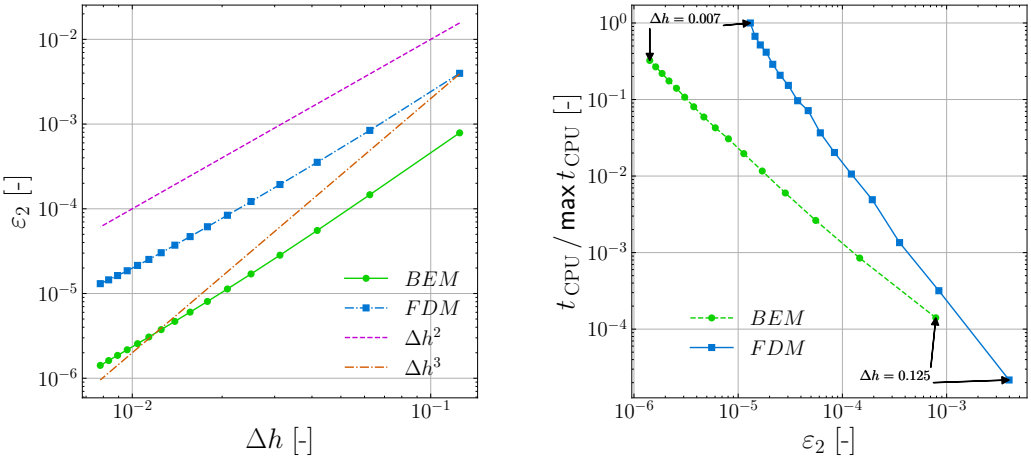

(a) (b)

Figure 2 : *Influence of spatial step* Δh *on* ε_2 *error for dimensionless* u (a) *and on the ratio* t_{CPU} *time and* ε_2 (b).

Firstly, the BEM method is verified on a case where an analytical solution is known. A rectangular domain is considered. Thus, for the flat wall case $\gamma(\mathbb{P}, y^\star) = 0$. Analytical solution u^a for Eq. (2) is used as a reference:

$$u^a(\boldsymbol{x}^\star) = (x^\star)^2 - (y^\star)^2.$$

The analytical solution is compared with the BEM one and the finite-difference method (FDM). The latter is implemented using JACOBI's method. For the comparison purpose, the error ε_2 is defined by:

$$\varepsilon_2 = \left|\left| u - u^a \right|\right|_2.$$

The results are computed for boundary and internal points. Different values of the spatial step Δh are chosen according to the total number of boundary elements N_e.

Figure 2(a) presents the error according the spatial step of each method. It highlights that BEM has a lower error compared to FDM results for all spatial step. Both approaches have an error proportional with Δh^2. Figure 2(b) gives the computational time ratio according to the error. Here the ratio is computed so that the maximal value is one for the method that requires the most computational resources. The Figure shows that for the same level of accuracy, the BEM is faster to compute the solution than the FDM.

3. Design optimization problem

The objective of this work is to improve energy efficiency of a building wall by finding the optimal shape of the left boundary which is in contact with outside environment. Thus, the optimization problem aims at finding parameters of the left boundary that minimizes a heat flux on the right wall:

$$\boldsymbol{p}^\circ = \arg\min_{\boldsymbol{p}\in\Omega_p} J. \tag{13}$$

In winter, the issue is to maximize the inward heat flux while in summer, it is the opposite. The objective function $J\left[\mathrm{W.m^{-2}}\right]$ is the total inward heat flux on the right boundary, corresponding to the inside of the building:

$$J = s\,\frac{1}{H}\int_0^H -k\,\boldsymbol{\nabla} T\,\vec{n}\,dy\,, \tag{14}$$

where s is the sign of the objective function depending on the different seasons. Namely, $s = 1$ and $s = -1$ in summer and winter, respectively. Note that the objective function needs to be minimized under several constraints. First, the physical volume of the wall $V_{\boldsymbol{p}}$ should not exceed the reference case V_∞. The reference case is defined as the flat standard wall ($\gamma = 0$ in Eq. (1)). Thus, the cost function Eq. (14) needs to be minimized under the following constraint:

$$V_{\boldsymbol{p}} \leq V_\infty,$$

which leads to

$$\int_{\Gamma_3} L\,d\Gamma - \int_{\Gamma_1} \gamma\,(\boldsymbol{p}\,,\,y)\,d\Gamma \leq \int_{\Gamma_3} L\,d\Gamma,$$

which can be rewritten as

$$\int_{\Gamma_1} \gamma\,(\boldsymbol{p}\,,\,y)\,d\Gamma \geq 0. \tag{15}$$

The second constraint that must be satisfied by the parametrized mapping is that the maximum width of the wall cannot be higher than L. In other words, the left and right boundaries cannot intersect each other:

$$\gamma\,(\boldsymbol{p}\,,\,y)\,d\Gamma \leq L - \delta, \tag{16}$$

where δ is a given spatial tolerance.

The cost function Eq. (14) is minimized with Constrained optimization by linear approximation method (COBYLA) [6]. It works by iteratively approximating the actual constrained optimization problem with linear programming problems.

4. Case study

4.1. Description

The case study considers a house wall in summer and winter conditions. The wall composed of bricks with thermal conductivity $k = 1\,\mathrm{W\,.\,m^{-1}\,.\,K^{-1}}$. The height and width of the wall are $H = 3\,\mathrm{m}$ and $L = 0.3\,\mathrm{m}$. For the mapping function γ Eq. (1), a third order polynomial is considered:

$$\gamma\,(\boldsymbol{p}\,,\,y) = p_0\,\frac{y}{H}\left(\frac{y}{H} - p_1\right)\left(\frac{y}{H} - 1\right).$$

The absorptivity of the right boundary is set to $\beta = 1$. The urban environment assumes a front building of 5 m height and placed at 3 m of the boundary Γ_1. The incident radiation flux are computed using analytical projections of the solar angle, considering shadow induced by front building and by the own shape of the boundary Γ_1. For the boundary Γ_3 of the wall, the temperature of the inside ambient air is $T_R = 20\,^{\circ}\mathrm{C}$. The number of boundary elements is set to $N_e = 256$, which corresponds to a dimensionless spatial step $\Delta h = 8.5 \cdot 10^{-3}$. The spatial tolerance is set to $\delta = 2\Delta h$.

4.2. Results

Table 1 : *Optimization results.*

	Scaled cost function		Optimized shape parameter		Volume of the wall		Computational cost	
Configuration	$J_f\,[-]$	$J_o\,[-]$	$p_0^\circ\,[-]$	$p_1^\circ\,[-]$	$V_f\,[-]$	$V_o\,[-]$	iter.	$t_{CPU}\,[\mathrm{s}]$
Summer	1	0.93	1.12	0.51	1.00	0.99	20	231
Winter	1	1.24	−1.13	0.49	1.00	0.81	22	241

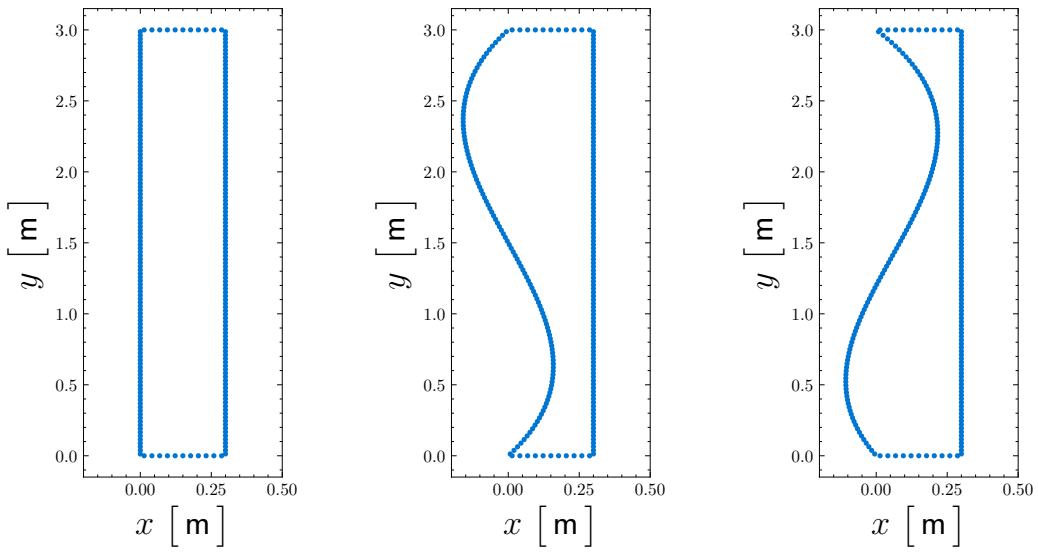

(a) (b) (c)

Figure 3 : *Flat wall shape* (a) *and optimized shapes of the wall in summer* (b) *and in winter* (c).

Shape optimization problem of building facade is solved using the method described in Section 3.The direct problem is solved for the summer (21^{th} August) and winter (21^{th} January) seasons. The radiation flux are generated using standard climate for the city of Perpignan, France. The flat wall is considered as reference case and denoted by subscript f. Table 1 provides the results for both configurations. The results show benefits for energy efficiency. The heat transfer is reduced by 7% in Summer and increased by 24% in Winter. Furthermore, the volume of the optimized shape are less than reference case (0.01%

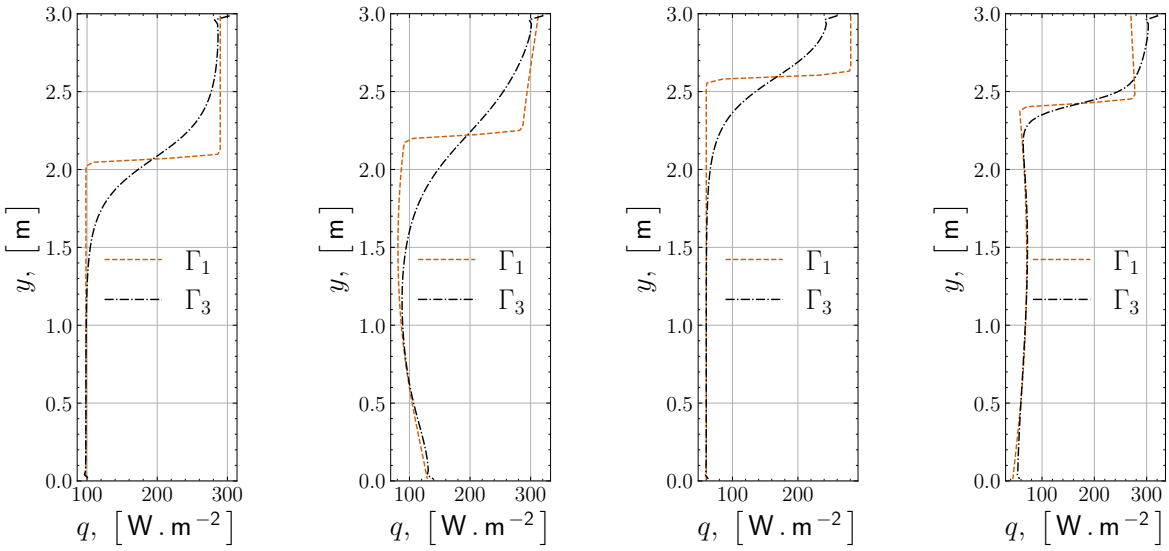

(a) summer / flat (b) summer /optimized (c) winter / flat (d) winter / optimized

Figure 4 : *Heat flux distribution along y axis on outside (Γ_1) and inside (Γ_3) boundaries.*

and 19% for summer and winter, respectively). Optimized design parameters are given Table 1 and illustrated in Figure 3. Figure 4 shows influence of the shape of the left boundary on the heat flux distribution along Γ_1 and Γ_3. According to the summer optimized shape, the wall has convexity on the higher part, which makes difficult for sun radiation to penetrate wall on that zone. Thus, total heat flux is lower in case of optimized design. Same logic can be applied for the optimized shape in winter. Due to concavity, distance to opposite wall is decreased. Thus, optimized shape shows an improvement of the global energy efficiency for increasing the heat transfer through the wall for both winter and summer periods.

5. Conclusion

This article investigates the use of BEM to solve a shape optimization problem of building walls. First the method is verified considering an analytical solution. It highlights that the approach is faster and more accurate than standard finite-difference method. Then, a case study is considered for optimization. The incident short-wave radiation flux is varying according to the height of the facade, due to shadow induce by the urban environment and by the own shape of the wall. Results show that for a reduced volume of the wall, energy efficiency can be improved by 13% and 100% in Summer and Winter respectively. Future works should focus on extending the methodology for transient heat transfer.

References

[1] J. Berger, S. Gasparin, W. Mazuroski, and N. Mendes. An efficient two-dimensional heat transfer model for building envelopes. *Numerical Heat Transfer, Part A: Applications*, 79(3):163–194, 2021. 1

[2] Inês Caetano, Luís Santos, and António Leitão. Computational design in architecture: Defining parametric, generative, and algorithmic design. *Frontiers of Architectural Research*, 9(2):287–300, 2020. 1

[3] M.N. Ozisik and H.R.B. Orlande. *Inverse Heat Transfer - Fundamentals and Applications*. CRC Press, New York, 2000. 2

[4] L. Marin. Numerical boundary identification for helmholtz-type equations. *Computational Mechanics*, 39:25–40, 12 2006. 4

[5] M. H. Aliabadi L. C. Wrobel. *The Boundary Element Method, Volume 1: Applications in Thermo-Fluids and Acoustics*. Wiley–Blackwell, 2002. 5

[6] M. Powell. A view of algorithms for optimization without derivatives. *Mathematics TODAY*, 43, 01 2007. 6